Plasma-induced formation of coatings on vegetable ivory microparticles immersed in silicone oil: Enhancing surface coverage using natural products

Yuri Ferreira da Silva, Giana Almeida, Anderson Thiago Vasconcelos Veiga, Renata Nunes Oliveira, Patrick Perré, Renata A Simao

To cite this article: Yuri Ferreira da Silva, Giana Almeida, Anderson Thiago Vasconcelos Veiga, Renata Nunes Oliveira, Patrick Perré, Renata Antoun Simao (2023): Plasma-induced formation of coatings on vegetable ivory microparticles immersed in silicone oil: enhancing surface coverage using natural products, Plasma Processes and Polymers, https://doi.org/10.1002/ppap.202300154

Article type: Research Article

Plasma-induced formation of coatings on vegetable ivory microparticles immersed in silicone oil: enhancing surface coverage using natural products

Yuri Ferreira da Silva[1,2], Giana Almeida[3], Anderson Thiago Vasconcelos Veiga[4,1], Renata Nunes Oliveira[5], Patrick Perré[2], Renata Antoun Simao[1]*

[1] Department of Metallurgical and Materials Engineering, Federal University of Rio de Janeiro, P.O. Box: 68505, 21945-970, Rio de Janeiro, RJ, Brazil

[2] Laboratoire de Génie des Procédés et Matériaux, CentraleSupélec, Université Paris-Saclay, SFR Condorcet FR CNRS 3417, Centre Européen de Biotechnologie et de Bioéconomie (CEBB), 3 rue des Rouges Terres 51110, Pomacle, France

[3] UMR SayFood, AgroParisTech, INRAE, Université Paris-Saclay, 91120, Palaiseau, France

[4] Department of Wood Science, Faculty of Forestry, The University of British Columbia, 2424 Main Mall, BC, V6T 1Z4, Vancouver, Canada

[5] Department of Chemical Engineering, Federal Rural University of Rio de Janeiro, Km 7 BR 465, 23890-000, Seropédica, RJ, Brazil

*Correspondence

Renata Antoun Simao, Department of Metallurgical and Materials Engineering, Federal University of Rio de Janeiro, P.O. Box: 68505, 21945-970, Rio de Janeiro, RJ, Brazil

Email: renata@metalmat.ufrj.br

Abstract

Aiming to enhance the potential applications of bioproducts, we developed an innovative approach for their hydrophobization using plasma activation of liquids. In this study, microparticles of vegetable ivory, a porous hygroscopic material, were treated by an air plasma jet while immersed in silicone oil. The in-liquid plasma treatment formed coatings that reduced particle water vapor sorption. Pore surface coverage and sorption reduction were enhanced by mixing silicone oil with copaiba oil-resin (*Copaifera spp.*). Mulateiro extract (*Calycophyllum spruceanum*) was not as effective, owing to a lower affinity with silicone oil. For the first time, we demonstrate the plasma-induced coating formation on particles immersed in liquid mixtures, a process in which liquid-liquid interfacial properties play a fundamental role.

Keywords: biopolymers; coatings; mannan; plasma jet; plasma-liquid interaction

1 INTRODUCTION

The ongoing illegal trade of ivory has brought African elephants close to extinction. According to a report from the International Union for Conservation of Nature (IUCN) published in 2021, African forest elephants (*Loxodonta cyclotis*) are critically endangered, that is, almost extinct in the wild.[1] Likewise, African savanna elephants (*Loxodonta africana*) are listed as endangered species.[2] The decline in African elephant population, highlighted in the 2016 African Elephant Status Report,[3] has been ascribed to the poaching for ivory,[4] which is still regarded as a high-value resource in China and other East Asian markets despite the international ban.

Within this framework, the seeds from *Phytelephas* palms, native of the southwestern Amazon, have risen as a sustainable alternative to ivory.[5,6] Their endosperm (**Figure 1**) has a similar color and texture to elephant ivory, what made them known as vegetable ivory. This porous, biodegradable and photoluminescent material[5,7,8] is mainly cultivated in Ecuador, with an estimated production of 100,000 metric tons per year.[9] The material is cut and carved

by local artisans to produce buttons, figurines, and other handcrafts, providing a source of income for rural communities.[10] The ecological appeal of vegetable ivory has also attracted attention of the fine-jewelry market, making it the centerpiece of the 2017 US Protagonists showcase curated by *Vogue Italia*.[11]

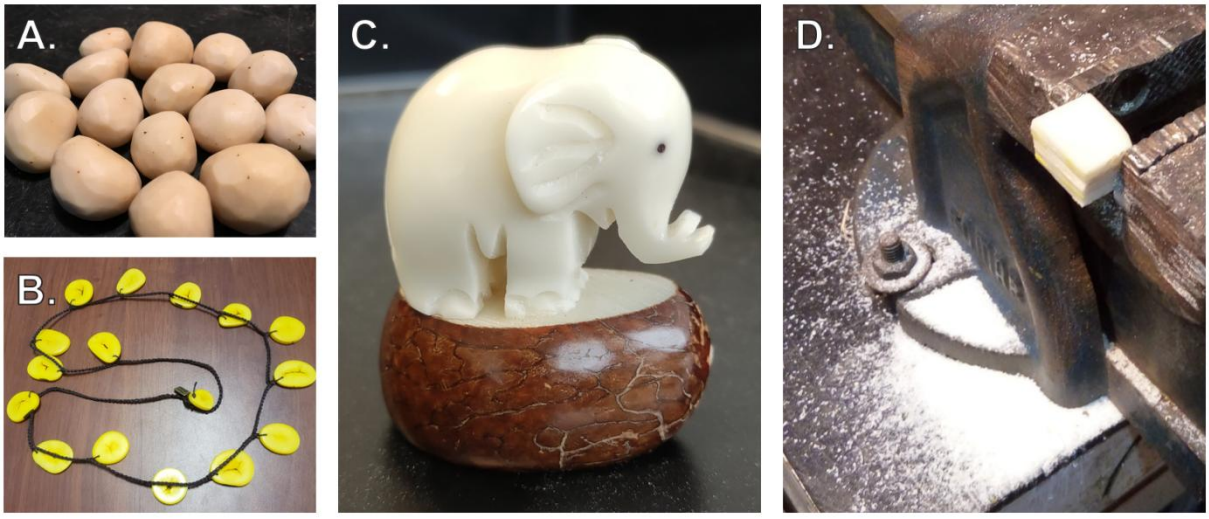

FIGURE 1. Endosperm of Phytelephas macrocarpa seeds (A). Jewelry produced with vegetable ivory disks (B). Vegetable ivory figurine in the shape of an elephant (C). Powder residue produced after cutting a vegetable ivory piece using a hacksaw (D).

As a subtractive manufacturing process, the production of vegetable ivory ornaments produces a powder residue which may correspond from 65 to 88% of the original material.[12] These particles have no current valorization strategy, and are a potential source of mannan, nanocellulose and pyrolysis products[9,12,13] owing to their high carbohydrate content (ca. 70 wt% homomannan and 7.5 wt% cellulose).[8,14] Also, the powder could be commercialized as an exfoliating agent for cosmetics,[15,16] providing a sustainable alternative against synthetic microbeads. Nevertheless, the abundant hydroxyl groups (OH) from the polysaccharide chains and the porous microstructure make vegetable ivory hygroscopic,[7] favoring its deterioration by micro-organisms.

On this basis, we introduce an innovative strategy for the hydrophobization of vegetable ivory microparticles by their plasma processing while immersed in silicone oil. Plasma activation of liquids such as water,[17] oils,[18,19] and their mixtures[20] has gained attention in the past few years as it induces the formation of reactive oxygen and nitrogen species (RONS), providing novel functionalities such as sterilizing and wound-healing properties to conventional liquids. In our approach, the reactive species provided by an atmospheric-pressure air plasma jet are used not only to modify the chemistry of the liquid, but also to induce the formation of coatings on the surface of the microparticles, i.e., plasma activation of silicone oil is used as a materials processing technique.

Hydrophobic coatings formed by plasma activation of silicone oil have already been reported for vegetable ivory,[7] glass,[21–23] and PMMA,[24] but the methods consist of crosslinking thin layers of the precursor on flat substrates. The in-liquid plasma processing poses no restrictions on sample geometry, allowing the modification of particles. Furthermore, the plasma jet induces a convective flow in the liquid,[19,25] enabling the uniform modification of particles with no need for stirring.

In addition to promoting environmental and economic benefits, plant origin products have demonstrated potential to confer novel characteristics to coatings,[26,27] such as electrochemical behavior,[28] antimicrobial activity,[29,30] corrosion resistance[31,32] and water repellence.[33,34] Copaiba oil, in particular, has been reported to enhance the antibacterial properties of coatings obtained by the plasma jet activation of silicone oil on vegetable ivory disks.[7] The oil-resin, extracted from the trunk of *Copaifera* trees, has been traditionally employed by indigenous peoples in the Amazon as a natural medicine due to its antimicrobial, anti-inflammatory and wound healing properties.[35,36]

On the flip side, silicone and copaiba oils are immiscible liquids, and their incompatibility affects the coating crosslinking rate.[7] In the present work, we further investigate the role of

liquid-liquid interfacial properties on coating formation during plasma jet activation. To this end, in addition to copaiba oil, mulateiro extract was evaluated as an additive to silicone oil owing to its distinct polarity. The extract of mulateiro bark (*Calycophyllum spruceanum*), known as the "tree of youth", has drawn attention of the cosmetics industry owing to its anti-aging, antimicrobial and anti-inflammatory properties.[37,38]

To assess coating formation, particle surface morphology was analyzed by Environmental Scanning Electron Microscopy (ESEM) and Atomic Force Microscopy (AFM). Chemical changes were characterized by Fourier Transform Infrared (FTIR) and Raman spectroscopies. The interfacial tension between the precursors was evaluated by pendant drop tensiometry. In addition, the effect of the plant origin precursors on surface coverage and water sorption was investigated by Raman imaging and Dynamic Vapor Sorption (DVS), respectively.

2 EXPERIMENTAL SECTION

2.1 Production of vegetable ivory microparticles

Phytelephas macrocarpa seeds (SisGen Code: AC591E1) were acquired from a local trader in Manaus (Brazil). The endocarp was removed by impact and the testa, the seed coat that covers the endosperm, was sanded using a 100-grit sandpaper (**Figure 2A**). Approximately 40 g of the endosperm was sliced using a hacksaw and then ground in an industrial blender (Spolu Attack, Spolu, Brazil) containing 200 mL of distilled water (Figure 2B). The grinding process was performed in 8 cycles of 30 s each, with an interval of 60 s between cycles to avoid sample overheating. At the end of the process, excess water was removed with a pipette and particles were cast on glass Petri dishes covered with aluminum foil, which were heated at 50ºC in an oven furnace for 24 h. Later, the particles were sieved and the fraction with

dimensions between 125 and 250 µm was selected (Figure 2D and 2E). The material retained on the 250 µm sieve was reprocessed using the same procedure described above.

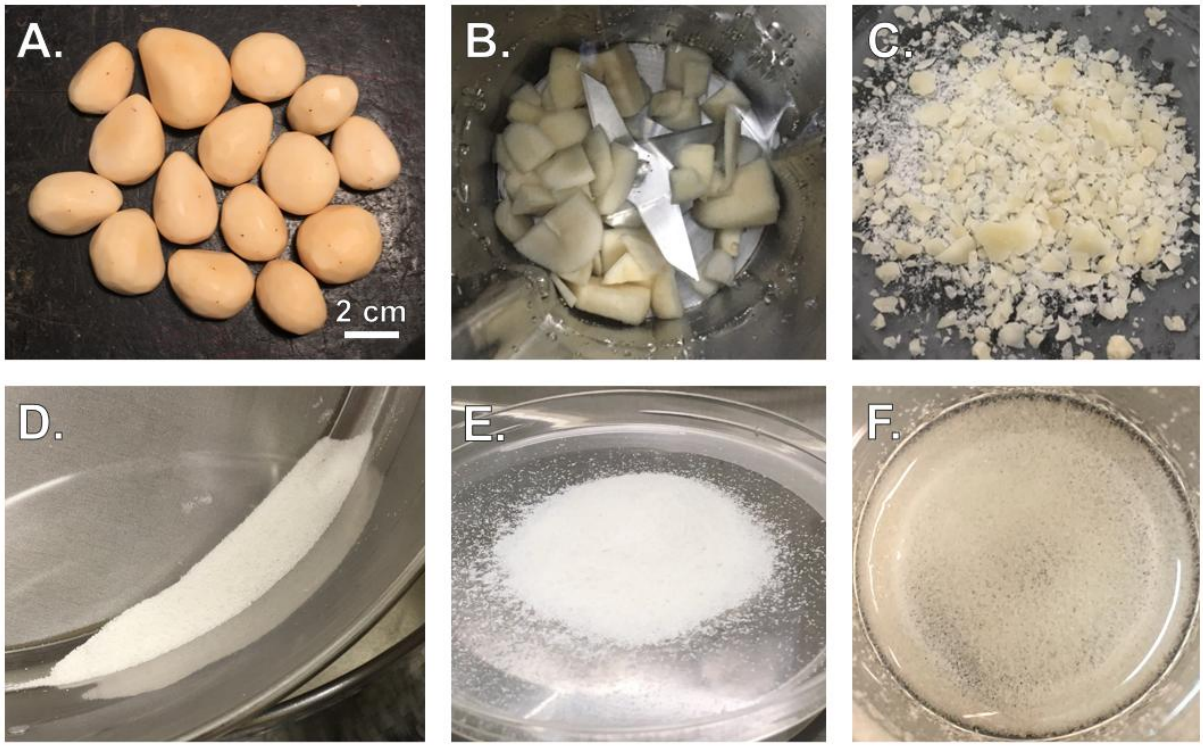

FIGURE 2. Endosperm of *Phytelephas macrocarpa* seeds (A). Vegetable ivory slices in industrial blender (B). Fragments obtained after grinding and drying (C). Particles with a diameter range between 125 and 250 µm obtained after sieving (D and E). Particles immersed in silicone oil (F).

2.2 Plasma treatment

In this process, three liquids were employed as precursors: silicone oil, copaiba oil (*Copaifera spp.*) and mulateiro extract (*Calycophyllum spruceanum*). Silicone oil was acquired from Vetec Química Fina (Rio de Janeiro, Brazil), whereas the plant-derived precursors were acquired in Mercado Adolpho Lisboa (Manaus, Brazil). Approximately 400 mg of vegetable ivory microparticles were immersed in 2 mL of the precursor liquid in a 25 mL beaker (Figure 2F). The following precursor liquid mixtures were tested: neat silicone oil, silicone oil /

copaiba oil (1:1 volume ratio) and silicone oil / mulateiro extract (1:1 volume ratio). Plasma activation of the liquids was performed with an atmospheric pressure cold plasma jet (PlasmaPen^{TM}, PVA TePla America, USA) fed with ambient air compressed at 700 kPa. According to the supplier, the system operates with a fixed 150 W power generator and the dimensions of the plasma plume vary between 1.2-1.5 cm in length and 0.5-0.6 cm in diameter. Before treatment, a 1.5 cm distance was established between the plasma jet nozzle and the surface of the liquid, which was further activated by the plasma jet for 30 s. After treatment, the particles were vacuum filtered and thoroughly washed with distilled water. Later, the material was cleaned in an ultrasound bath in distilled water for 15 min. Finally, the particles were once again washed, vacuum filtered, heated in an oven furnace at 50 ºC for 20 min and subsequently stored in desiccator containing silica gel for at least 24 h before characterization.

2.3 Environmental Scanning Electron Microscopy (ESEM)

Samples were analyzed in an environmental scanning electron microscope (Quanta 200, FEI, USA) using low vacuum mode (107 Pa), which allows non-conductive samples to be imaged without coating. Samples were fixed on an aluminum stub for scanning electronic microscope using a carbon double-side tape. Accelerating voltage was set at 13 kV while the working distance was varied between 7.5 and 8 mm.

2.4 Atomic Force Microscopy (AFM)

AFM images were acquired in an Alpha 300R (Witec, Germany) equipment in intermittent contact mode. Topography and phase contrast images were scanned over 20 x 20 μm^2 regions,

and the results were processed in Gwyddion software (version 2.58).[39] Image processing consisted in levelling by mean plane subtraction, alignment of rows by a second order polynomial, scars correction and application of a 2-pixel Gaussian filter.

2.5 Fourier Transform Infrared Spectroscopy (FTIR)

FTIR spectra of the precursor liquids and the microparticles were acquired in a Thermo Scientific Nicolet 6700 spectrometer employing an attenuated total reflectance (ATR) accessory. Absorbance spectra were registered in a range from 650 to 4,000 cm^{-1} with a resolution of 4 cm^{-1} and a total of 64 accumulations. The spectra, acquired in duplicate, were averaged, baseline corrected, normalized and smoothed (adjacent-averaging, 7 pts) in *OriginPro 8* software.

2.6 Raman Spectroscopy

Microparticles were analyzed in an Alpha 300R Plus (Witec, Germany) equipment using a 10 x objective lens (EC Epiplan Neofluar, ZEISS) with a numerical aperture of 0.25. Hyperspectral maps were acquired using a 785 nm laser with 20 mW power and a 600 g/mm grating. The chemical images, corresponding to a 100 x 100 μm^2 scanning area, consist of a total of 50 x 50 points with an integration time of 0.5 s. Average spectra corresponding to these regions were baseline corrected and normalized according to the intensity of the 890 cm^{-1} peak in *OriginPro 8* software. In addition, single spectra were generated in duplicate for the precursor liquids using an integration time of 0.5 s and 200 accumulations. Hyperspectral data were processed in RStudio (R version 4.1.3)[40] using the hyperSpec package.[41] Spectra were smoothed using a second order 9-point Savitsky-Golay filter and normalized by the Standard

Normal Variate (SNV) method. To plot average intensity maps for selected peaks (492, 890 and 1615 cm^{-1}), adjacent regions were selected, e.g., 1600-1630 cm^{-1}, and a linear baseline correction was performed before generating the chemical images.

2.7 Dynamic Vapor Sorption (DVS)

Moisture sorption isotherms were obtained at 25ºC in a dynamic vapor sorption analyzer (DVS-HT, Surface Measurement Systems, UK) using dry nitrogen as a carrier gas. Sample mass variation was recorded with a microbalance upon changing chamber relative humidity (RH) from 0 to 90 % with intervals of 10 % between RH levels. Each humidity level was kept constant until the rate of mass change per minute (dm/dt) was lower than 0.002 % per minute over a 15-min period. Equilibrium moisture content (EMC) was calculated using the dry mass obtained at the end of the first RH level (0% RH). Measurements were performed in duplicate, as illustrated in Supporting Information (Figure S1). The average difference between replicate EMC values, including adsorption and desorption, was below 10 and 2 % for untreated and plasma-treated samples, respectively. Furthermore, hysteresis was calculated upon subtracting EMC values obtained for desorption and adsorption for the same RH level.

The experimental data obtained from the moisture sorption isotherms was fitted to Guggenheim, Anderson and De Boer (GAB) model using a custom routine coded in RStudio (R version 4.1.3), in which the residual sum of squares (RSS) between the experimental data and the model curves was minimized employing the Nelder-Mead method. R^2 values higher than 0.99 were obtained for all curves and the RSS was of the order of 10^{-5}.

2.8 Measurement of precursor liquid interfacial tension

The interfacial tension between silicone oil and the plant-derived precursors was determined by pendant drop tensiometry, in which droplets were dispensed inside silicone oil in a quartz cuvette. Liquid density was determined by weighing using an analytical balance. As copaiba oil presented a lower density (0.933 g/cm^3) in comparison to silicone oil (1.007 g/cm^3), measurements were performed using an inverted needle. Drop volume was approximately 2 µL. In turn, mulateiro extract (1.017 g/cm^3) was dispensed using a regular needle (~ 50 µL). Drop shape was recorded using a Ramé-Hart 500 F-1 goniometer and processed in DropImage software. A total of 100 measurements were performed for each droplet with an interval of 0.2 s. This procedure was performed in duplicate. Interfacial tension data was calculated in Drop Image software according to Young-Laplace equation.[42]

3 RESULTS AND DISCUSSION

3.1 The morphology of vegetable ivory microparticles

ESEM images of vegetable ivory microparticles are presented in **Figure 3**. The particles present an angular shape, which may be associated with the anisotropic behavior of the endosperm together with the cellular structure of the porous medium. During the grinding process, cracks propagate preferentially along the elongated cells and necessarily also across the cells, for which the fracture surface confirms a brittle behavior. As illustrated in Figure 3, the endosperm pores, tubular in shape, present a near-parallel alignment. These pores are interconnected by smaller tubules with a few micrometers in diameter, as highlighted in Figure 3F.

It was already reported in literature that cracks formed in vegetable ivory endosperm propagate preferentially along the tubules in order to minimize fracture energy.[5] A similar

pattern can be observed in Figure 3C, 3D and 3E, in which particle borders coincide with near parallel planes formed by former tubules. As the pores are organized in an anisotropic structure consisting of concentric rings throughout the endosperm,[5,43] it is not surprising that the grinding process results in elongated particles, whose lengths were, in average, longer than the mesh used in the sieving process (250 µm). Sieving was then only efficient for selecting particle diameter.

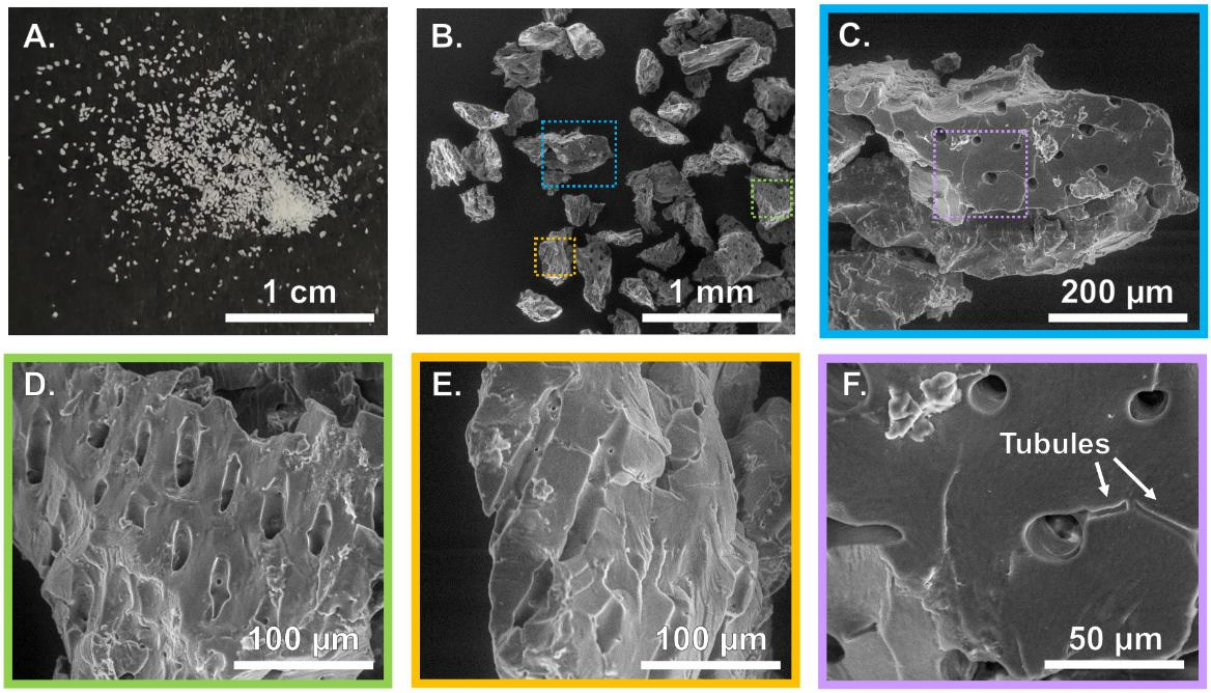

FIGURE 3. Microparticles of vegetable ivory (A). ESEM images of the microparticles with different magnifications: 100 x (B), 500 x (C), 1000 x (D and E) and 2000 x (F). Higher magnification images (C, D, E and F) correspond to the regions highlighted in B and C, as assigned by color.

3.2 Coatings formed during the liquid phase plasma treatment

Figure 4 presents ESEM images for microparticles after liquid phase plasma treatment. As illustrated in the insets, the treatment in silicone oil did not alter particle color, while copaiba

oil and mulateiro promoted subtle color changes to yellow and red, respectively. The color changes indicate the retention of chemical moieties from the natural precursors on the particle surface after plasma treatment. Upon analysis of the ESEM images, it is possible to observe that precursor liquid activation by the plasma jet resulted in the formation of coatings of substantial thickness on the particle surface. The layer is sufficient to cover the pores and cracks existing in untreated particles. These coatings are chemically stable in water, as the particles were abundantly washed and sonicated after plasma treatment. While the silicone-derived film is more uniform and follows the original surface features, the films obtained for the natural precursor mixtures present a heterogeneous structure with wavy patterns.

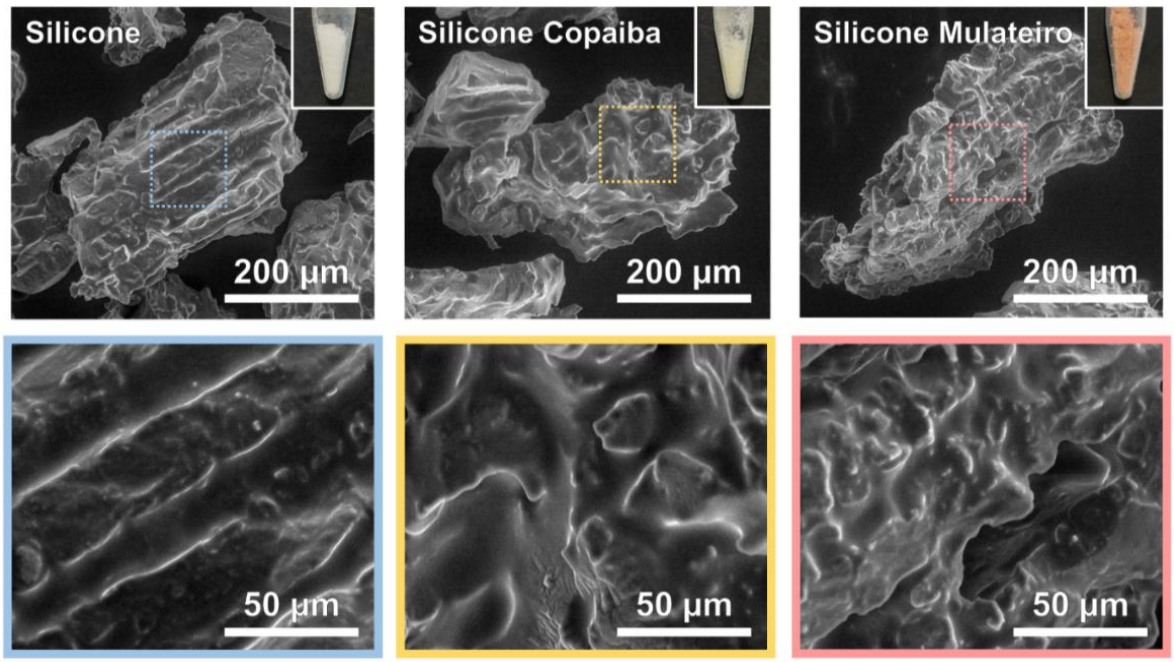

FIGURE 4. Microparticles of vegetable ivory coated by plasma jet activation of silicone oil, silicone oil / copaiba oil (1:1 volume ratio) and silicone oil / mulateiro extract (1:1 volume ratio). The highlighted regions correspond to the area shown in the higher magnification images (2000 x), as assigned by color. Insets: microparticles in Eppendorf tubes.

The formation of coatings on the particles surface is substantiated by AFM results, presented in **Figure 5**. The surface of untreated vegetable ivory microparticles presents a rough and heterogeneous topography, presenting granular structures with dimensions varying from the

nanometer to micrometer ranges. These features may correspond to crystalline mannan I, which occurs in vegetable ivory as an encrusting substance in a skeleton consisting of mannan II and cellulose microfibrils.[44] Moreover, depressions can be observed over the surface, which may be associated with micrometric tubules of the anatomical structure and cracks formed during the grinding process. The phase contrast image demonstrates the chemical homogeneity of the material in the analyzed scale and point out the presence of deposits of a more rigid phase (dark color) over the sample surface. This material could correspond to inorganic compounds naturally present in the endosperm, such as silica (SiO_2) or metallic impurities attached to the samples during the grinding process.

The particles treated by plasma in silicone oil presented a smoother and more homogeneous surface with respect to the untreated sample, in accordance with the coating formation observed by ESEM. This result is similar to that reported for air plasma jet crosslinked coatings in vegetable ivory, although obtained by a different method.[7] Moreover, a few nanoparticles of softer material could be observed on the coating surface, probably associated with impurities present in the commercial silicone oil. The mixtures containing plant-derived precursors resulted in an increase in phase heterogeneity in comparison to the silicone-derived coating, which confirms the ESEM observations. These AFM images reveal the incorporation of chemical moieties from both precursors to the formed coatings. In particular, the intensity of the phase contrast scale was higher for copaiba oil in comparison to mulateiro extract, indicating a higher incorporation of the former precursor into the coating structure.

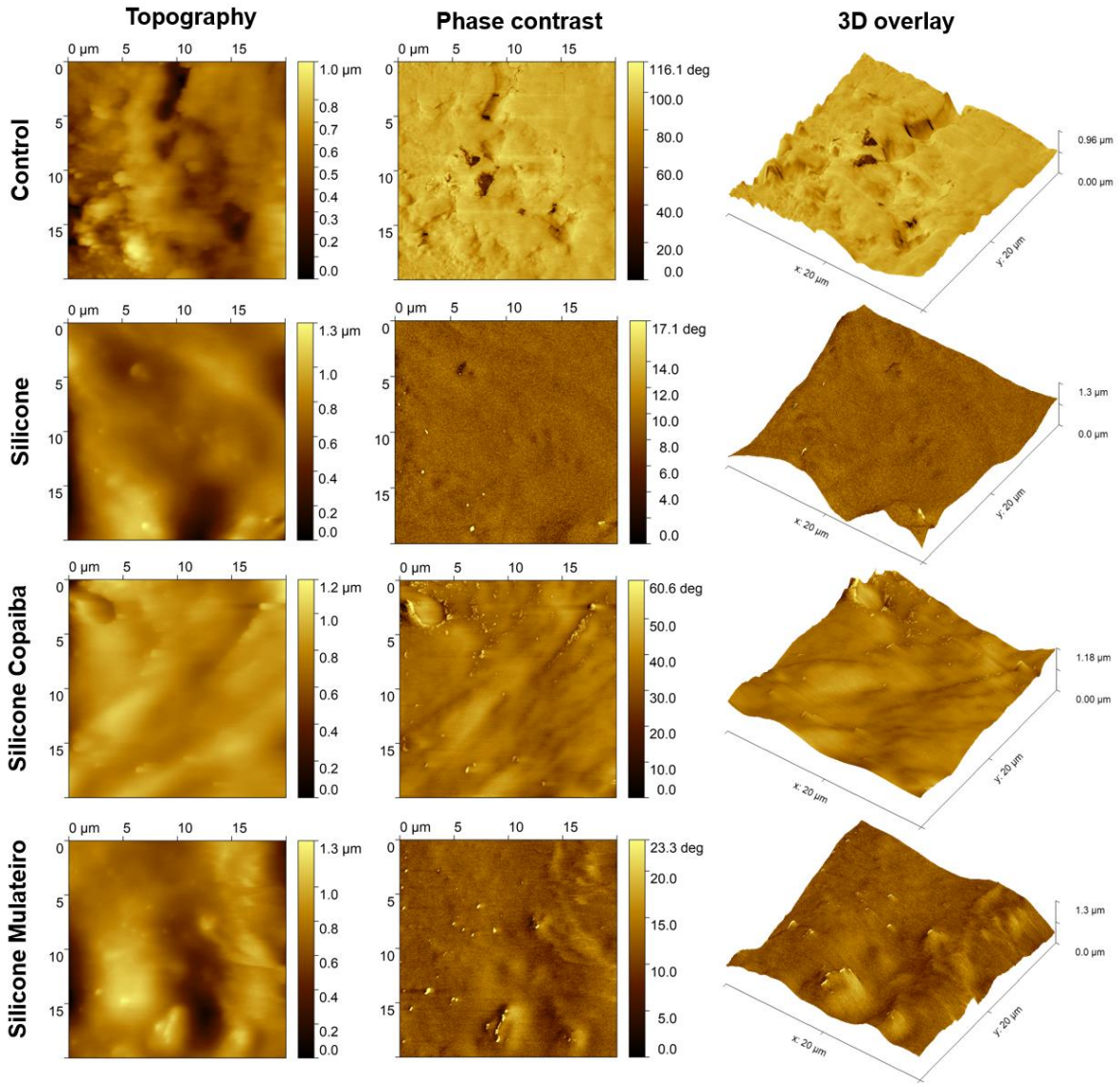

FIGURE 5. Atomic force microscopy images (20 x 20 μm^2) of vegetable ivory microparticle surface before and after liquid phase plasma treatment.

3.3 The interaction between plasma, precursor liquids and the microparticles

Cold air plasma is obtained upon the ionization of its main constituents, nitrogen (~ 78 %) and oxygen (~ 21 %) molecules, by electron impact dissociation. As a result, several reactive species are generated, e.g., atomic oxygen (O), atomic nitrogen (N), excited oxygen molecules (O_2^*), excited nitrogen molecules (N_2^*), ozone (O_3) and nitrogen oxides (N_xO_y).[45]

These reactive oxygen and nitrogen species (RONS) impact the surface of the liquid in addition to electrons, neutrals and radiation, forming a plasma-liquid interface with a micrometric extent.[19,46] In this interface, reactions between the plasma energetic species and the molecules of the liquid occur. The long-lived species generated by these reactions are further distributed throughout the bulk of the liquid by convective transport[25,47] and, upon reactions on the particle surface, may form the coatings observed by ESEM (Figure 4) and AFM (Figure 5) techniques.

As indicated by the AFM results, mixing silicone oil with copaiba oil or mulateiro extract affects coating phase heterogeneity to different extents. This result may be associated with the interaction between the liquids, as illustrated in **Figure 6**. Both plant precursors phase-separate in silicone oil (Figure 6A), but copaiba oil exerts a lower interfacial tension (1.60 ± 0.01 mN/m) in comparison to mulateiro extract (5.62 ± 0.15 mN/m).

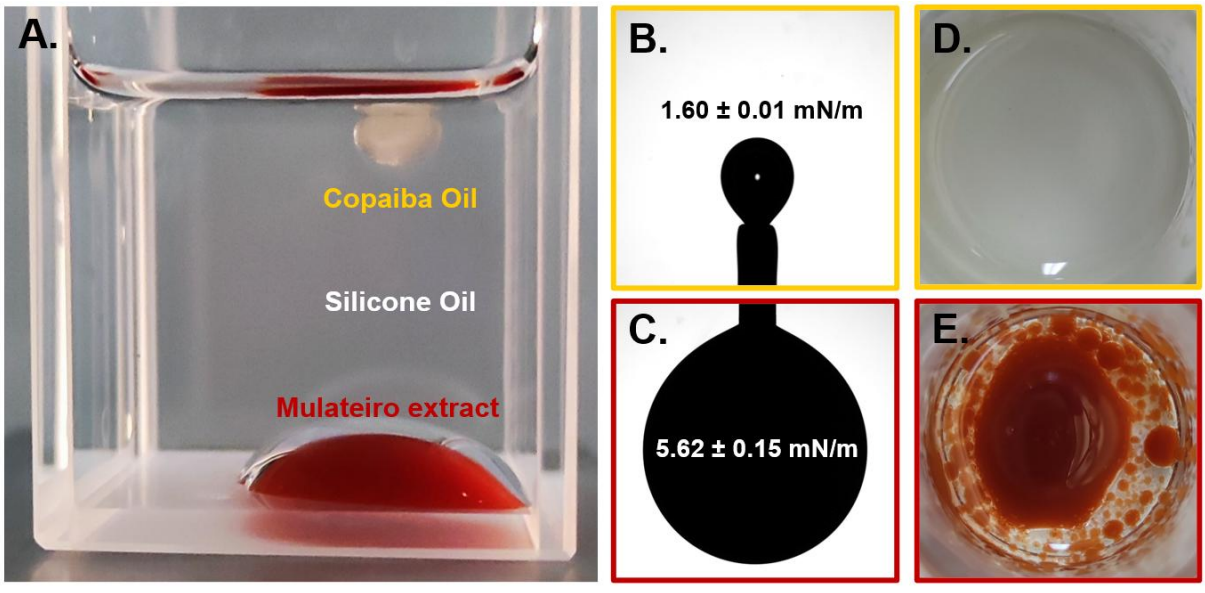

FIGURE 6. Copaiba oil and mulateiro extract drops immersed in silicone oil (A). Interfacial tension of copaiba oil (~ 2 µL) (B) and mulateiro extract (~ 50 µL) (C) droplets in silicone oil. Mixtures of copaiba oil (D) and mulateiro extract (E) with silicone oil after stirring.

The plasma jet, fed by air compressed at 700 kPa, exerts a convective flow in the liquid,[19,47] as illustrated by the formation of an air cavity in **Figure 7B and 7C**. The convection enables the transport of chemical species generated in the plasma-liquid interface to the bulk of the liquid and imposes shear stresses on the dispersed phase droplets. The droplets can be deformed and ruptured if the hydrodynamic stresses imposed by silicone oil overcome interfacial tension. Assuming that viscous forces are dominant, i.e., laminar flow, the ratio between viscous and interfacial stresses can be quantified by the capillary number (Ca), expressed as $\mu GR/\gamma$. In this equation, μ is the viscosity of the continuous phase, G is the local extensional rate experienced by the droplet, R is the droplet radius and γ is the interfacial tension.[48] Ca, a dimensionless quantity, is related to the extent of deformation experienced by the droplets.

On this basis, copaiba oil would form smaller droplets in silicone oil in comparison to mulateiro extract, owing to the lower interfacial tension. This is illustrated in Figure 6D and 6E, in which a translucid aspect was obtained after stirring the silicone copaiba mixture, whereas coalesced drops are observed for mulateiro extract. The reduced droplet size increases the interfacial area between copaiba oil and silicone oil and may favor the incorporation of organic moieties to the coating structure, as indicated in the AFM images.

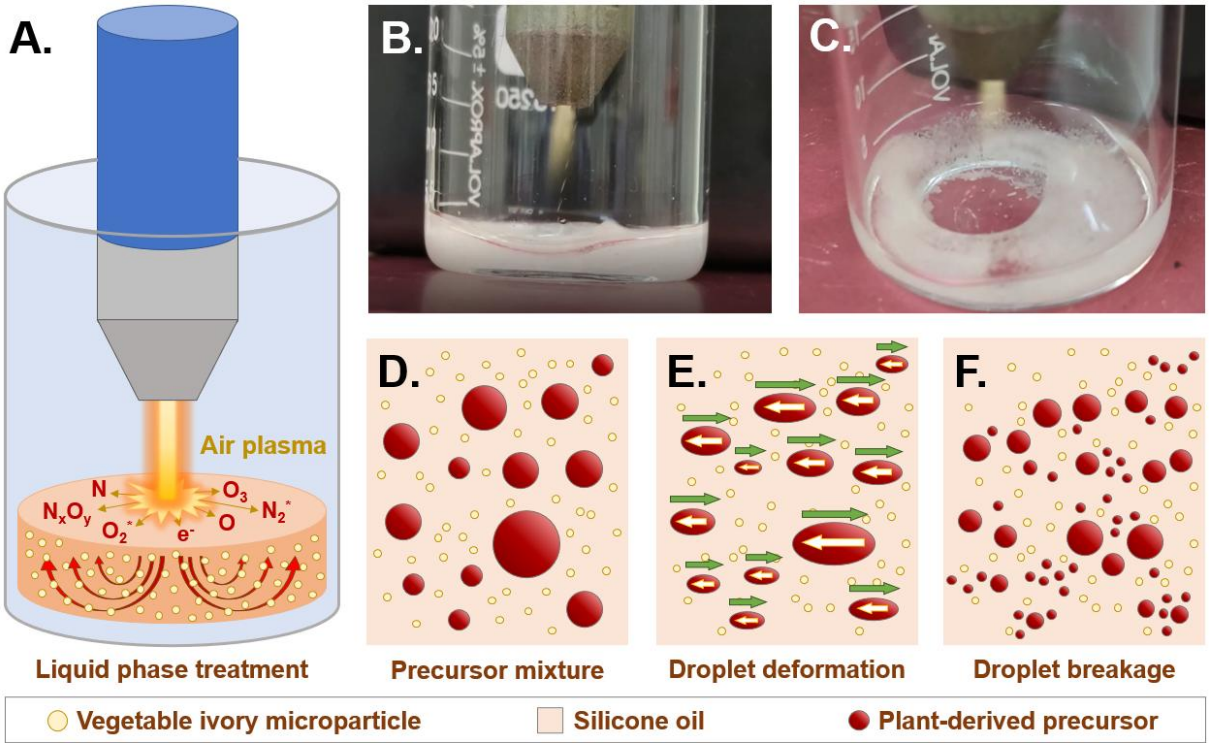

FIGURE 7. Schematic diagram of air plasma activation of a precursor liquid and examples of the generated RONS species (A). Plasma jet activation of silicone oil containing vegetable ivory microparticles (B). Photograph illustrating the formation of an air cavity as a result of the convective flow exerted by the plasma jet (C). Schematic diagrams illustrating the formation of a heterogeneous mixture by silicone oil and the plant-derived precursors (D), in which droplet deformation (E) and breakage (F) occur as result of viscous shear stresses during plasma treatment.

3.4 Spectroscopy analyses of the plasma treated particles by FTIR and Raman

The interfacial properties of the liquids are related to their chemical composition, as illustrated by the spectroscopy analyses summarized in **Figure 8**. Detailed peak assignments are available as Supporting Information in Tables S1 to S4. Silicone oil consists of Si-O-Si chains abundant in CH_3 side groups, which confer a non-polar character to the liquid. Copaiba oil, in turn, presents vibrations from both polar (C=O) and non-polar compounds (CH_2, CH_3, β-caryophyllene), indicating an intermediate polarity. On the other hand, mulateiro extract is

abundant in OH groups, which are polar. The background signal observed in the Raman spectrum of the extract may be a result of laser-induced fluorescence (LIF)[49] emitted by unsaturated (C=C) conjugated systems. The differences in polarity correlate with the higher interfacial tension (Figure 6) between mulateiro extract and silicone oil in comparison to copaiba oil.

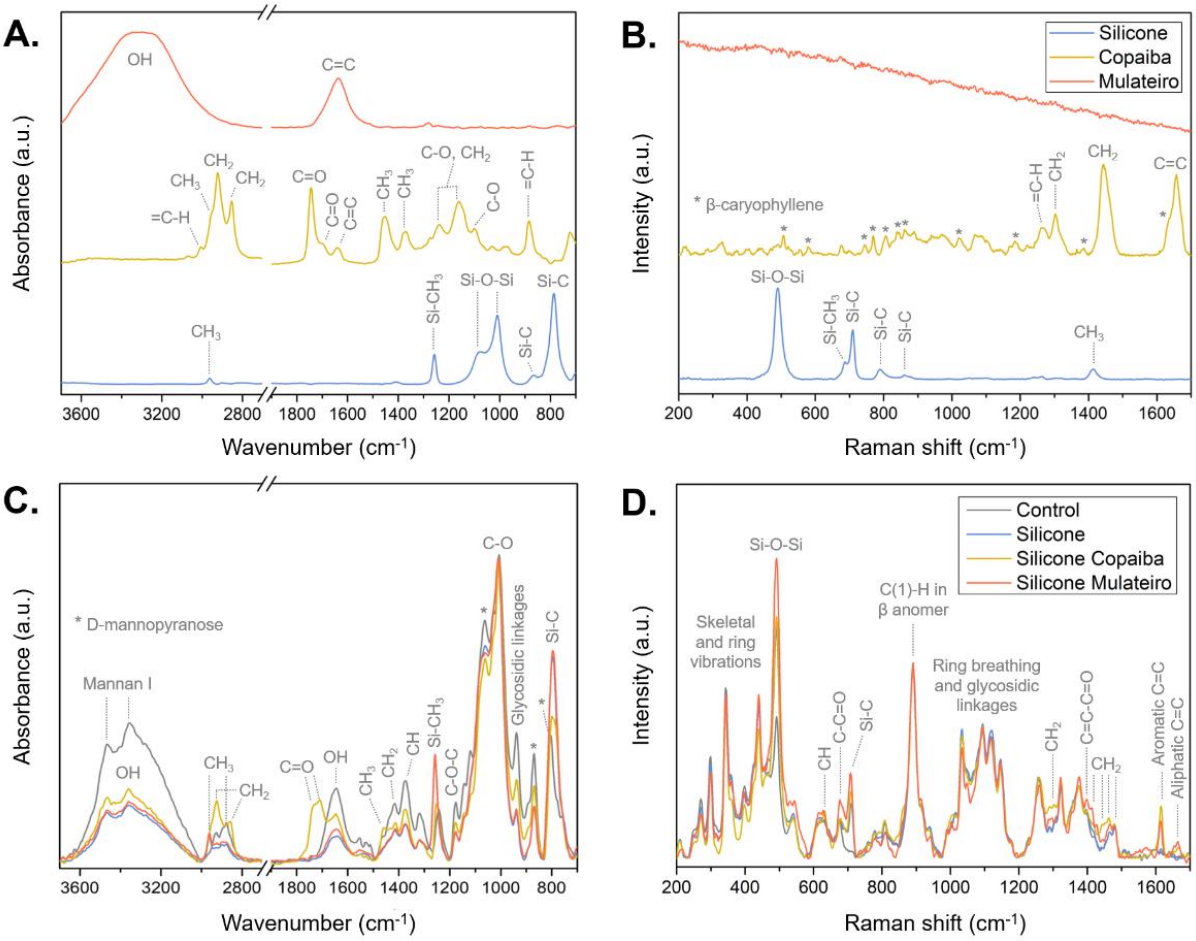

FIGURE 8. FTIR and Raman spectra of precursor liquids (A and B) and vegetable ivory microparticles (C and D) before (control) and after plasma treatment.

After plasma treatment of the microparticles, the intensity of mannan-related peaks (Figure 8C and 8D) was attenuated due to the presence of the coatings. Characteristic vibrations of silicone oil were observed for all samples both in FTIR (CH_3, Si-C, Si-CH_3) and Raman (Si-O-Si, Si-C) spectra, demonstrating the formation of a silicone-like structure. In particular, the

786 cm^{-1} peak (Si-C in Si-$(CH_3)_1$) was shifted to 796 cm^{-1}, indicating a higher amount of Si-$(CH_3)_2$ bonds,[50,51] i.e., the predominance of CH_3 side groups over CH_3 terminal groups, characteristic of a crosslinked structure. This result is substantiated by the absence of the 866 cm^{-1} peak (Si-C in Si-$(CH_3)_3$). In essence, the plasma treatment may have promoted the demethylation of polydimethylsiloxane (PDMS) chains[24,52–54] in terminal Si atoms, forming CH_3^+ and $(CH_3)_3SiO[Si(CH_3)_2O]_nSi(CH_3)_2^+$ macroradicals which were crosslinked on the particles surface.

Mixing silicone oil with copaiba oil or mulateiro extract affects the organic character of the plasma crosslinked structure. This is demonstrated by the Si-C (710 cm^{-1}) / Si-O-Si (492 cm^{-1}) intensity ratio in the Raman spectrum, which is increased from 0.23 (silicone) to 0.28 for both mixtures. Nevertheless, a higher diversity of functional groups was retained or formed from the silicone copaiba oil mixture. For instance, new peaks could be observed in the FTIR spectrum at 1733 (ester C=O) and 1710 cm^{-1} (ketone C=O), with an increased 1710 / 1733 cm^{-1} ratio in comparison with the precursor. The increase in ketone groups could be attributed to hydrogen abstraction[55] from copaiba oil compounds and further reaction with atomic oxygen (O) provided by the air plasma jet.

Moreover, the FTIR spectrum demonstrates a greater incorporation of CH_3 (2952, 1458 cm^{-1}) and CH_2 (2925, 2856 cm^{-1}) groups to the coating structure in comparison to the silicone sample. Peak intensity increases associated with CH_2 were also observed in the Raman spectrum (1302, 1443 and 1464 cm^{-1}), and new peaks could be identified at 630, 1615 and 1665 cm^{-1}. The 630 (C-H out of plane bending) and 1615 cm^{-1} (aromatic ring stretching) demonstrate the formation of aromatic rings as a result of the plasma treatment. These functional groups may have been formed after breakage of π bonds[19] from aliphatic unsaturated compounds in order to form structures with higher stability. This is substantiated by the 1665 cm^{-1} peak (aliphatic C=C), lower in comparison to the precursor, indicating a low retention of aliphatic structures after plasma treatment.

The FTIR spectrum for the silicone mulateiro sample was nearly identical to the silicone sample, except for subtle increases in the OH band (3700-3000 cm^{-1}) and the OH bending peak (1645 cm^{-1}). The similarity suggests a low incorporation of mulateiro-derived moieties to the coating structure, as indicated by AFM. Nevertheless, intensity increases at 675 (C-C=O), 1400 (C=C-C=O) and 1412 cm^{-1} (CH_2) occurred in the Raman spectrum. Likewise the copaiba sample, peaks corresponding to aromatic (1615 cm^{-1}) and aliphatic (1665 cm^{-1}) C=C were also present, indicating that similar reaction pathways may occur during the treatment. In particular, C-C=O and C=C-C=O groups may have been formed by hydrogen abstraction and/or π bond breakage mechanisms, as discussed for copaiba oil.

The affinity between the precursors affects the coating composition. A lower interfacial tension with silicone oil favors the incorporation of moieties from the natural precursor into the coating structure. In order to evaluate whether these changes in coating structure affect the compatibility with the particles, chemical images were generated by Raman imaging.

3.5 Visualization of microparticle chemical composition by Raman imaging

Raman imaging results are summarized in **Figure 9**. The 492, 890 and 1615 cm^{-1} peaks were selected as markers for silicone-like material (Si-O-Si stretching), mannan (anomeric C(1)-H bending) and C=C stretching in aromatic rings, respectively.

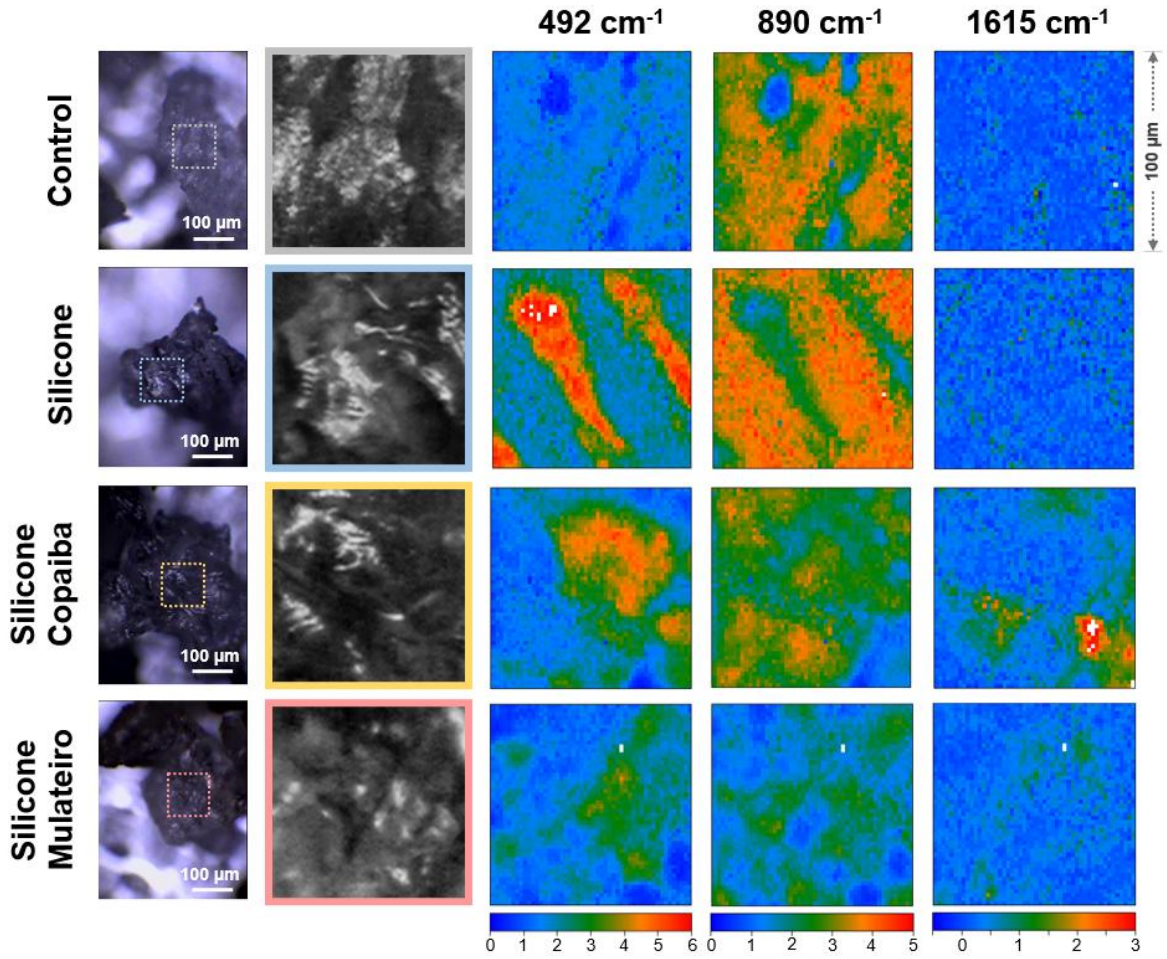

FIGURE 9. Optical microscopy images acquired in the Raman confocal microscope (left) and hyperspectral maps (right, 100 x 100 µm^2) of the highlighted colored regions. The scale for the maps corresponds to the average spectral intensity at 492 cm^{-1} (Si-O-Si bonds), 890 cm^{-1} (anomeric C(1)-H bending in mannan) and 1615 cm^{-1} (aromatic C=C stretching), respectively.

As expected, the untreated sample (control) is abundant in mannan and no signal was detected in the pores, large enough to reduce the signal (tens of micrometers as shown in Figure 3). The sample treated in silicone oil depicts well-defined regions abundant in silicone-like material, probably corresponding to pores. It is worth noting that the intensity of the remainder area, corresponding to mannan, was not affected. This result highlights the lack of chemical affinity between the silicone-like material (non-polar) and the hydroxyl-rich, polar substrate.

The natural precursors enhanced the chemical affinity between the plasma-crosslinked material and the substrate. For both copaiba oil and mulateiro extract, the silicone-like

material (492 cm^{-1}) was more evenly distributed on the sample surface, probably due to the increase in organic character observed by Raman spectroscopy (Figure 8D). Furthermore, the precursor mixtures reduced the average intensity of the 890 cm^{-1} peak throughout the analyzed region, indicating an increase in surface coverage. This effect was more pronounced for mulateiro extract, due to the formation of thicker coatings. Regarding aromatic groups (1615 cm^{-1}), their presence was more evident in the silicone copaiba sample, substantiating the lower incorporation of mulateiro-derived moieties to the coating structure.

Spectroscopy analyses (Figure 8) demonstrated that mulateiro extract is abundant in polar functional groups, while copaiba oil contains both polar and nonpolar moieties. On this basis, copaiba oil could present an intermediate polarity, i.e., affinity with the polar polysaccharide substrate and silicone oil (non-polar). As a result, the oil-resin acted as an interfacial agent during the plasma treatment, enhancing the penetration of the precursor mixture into the sample pores. This result is similar to the obtained for a different method.[7] On the other hand, mulateiro extract may not have induced the same effect due to the incompatibility with silicone oil. As a consequence, most of the precursor mixture was crosslinked on the particle surface, forming thicker coatings. These differences in surface coverage and pore filling may affect the mass transfer properties of the particles, which were evaluated by DVS.

3.6 The effect of the coatings on the interaction between vegetable ivory and water vapor

Moisture sorption isotherms for vegetable ivory microparticles are shown in **Figure 10A**. The samples presented isotherms with a sigmoidal shape (IUPAC Type II), characteristic of a monolayer-multilayer sorption mechanism.[56]

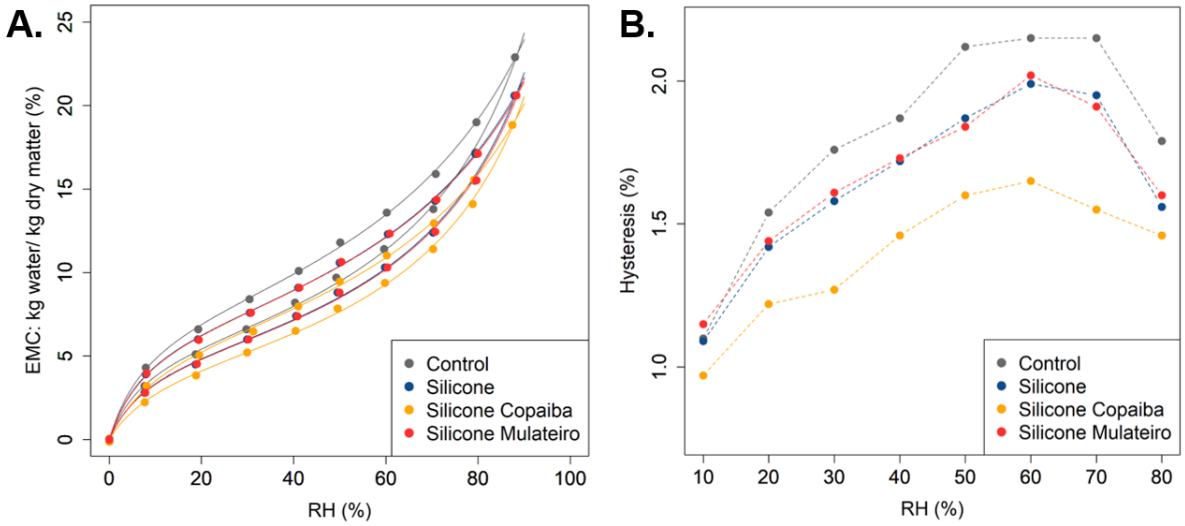

FIGURE 10. Sorption-desorption isotherms obtained at 25ºC for vegetable ivory microparticles, in which solid lines correspond to the data fitted by the GAB model (A), hysteresis data calculated from the envelope curves (B).

At low RH values, the slope of the isotherm corresponds to the formation of a monolayer of water molecules which strongly interact with primary sorption sites in the material. After completion of the monolayer, sorption rate is decreased and the slope is reduced, corresponding to the continuous assembly of water multilayers. The final section of the isotherm, convex to the RH axis, presents an increased sorption rate which may be associated with liquid condensation in micropores and the softening of amorphous domains occurring at high RH.[57] Monolayer-multilayer sorption is substantiated by the C and K values obtained from the GAB model (**Table 1**). As $C >> 1$ and $K \approx 1$, monolayers and multilayers are distinct from each other, but multilayers behave closely to a bulk liquid.[58]

TABLE 1. Parameters obtained from the GAB model

	Adsorption			***Desorption***		
Sample	**X_m**	**C**	**K**	**X_m**	**C**	**K**
Control	0.059	14.957	0.844	0.079	15.619	0.753
Silicone	0.054	13.950	0.843	0.071	16.096	0.755
Silicone Copaiba	0.049	10.619	0.849	0.064	12.133	0.768
Silicone Mulateiro	0.054	13.769	0.840	0.072	15.749	0.750

The amount of adsorbed water by kg of dry material, which can be as high as 20% for large RH values (> 80%), is comparable to other lignocellulosic materials[59–61] and demonstrates the great hygroscopicity of vegetable ivory. In polysaccharides such as mannan and cellulose, the main sorption sites for water vapor are hydroxyl (OH) groups. As crystalline domains are closed to water sorption, only the sorption sites present in amorphous regions and at the surfaces of crystals are available for interaction.[62] Vegetable ivory is constituted by a skeleton of mannan II (semicrystalline) and cellulose microfibrils encrusted with mannan I (crystalline) grains.[44] In this sense, most of the available sorption sites in the material could be present in the amorphous regions of mannan II and at the surfaces of mannan I crystals and cellulose microfibrils.

The coatings reduced the accessibility to sorption sites in vegetable ivory and, consequently, decreased the equilibrium moisture content (EMC) throughout the analyzed RH range. This result is demonstrated by the X_m parameter from the GAB model (Table 1), which is an indicator of the availability of sites for water sorption in the material.[58] The silicone and silicone mulateiro coatings presented the same X_m, demonstrating that mulateiro extract did

not affect the surface coverage of hydroxyl groups by the silicone coating. This effect can be visualized in Figure 10A, in which the curves for these samples coincide. On the other hand, an evident decrease in water sorption was observed for the silicone copaiba mixture, alongside a reduction in the X_m parameter.

The particles with the silicone copaiba coating also presented the highest reduction in sorption hysteresis (Figure 10B) (Hysteresis at a given RH = $EMC_{des} - EMC_{ads}$). One theory dealing with moisture sorption hysteresis has attributed it to the stress relaxation of amorphous polymers favored by their softening promoted by swelling.[57,60] As the coatings reduced the accessibility of water to the sorption sites into the material, swelling might have been reduced, resulting in a lower hysteresis effect.

The greater reduction in equilibrium moisture content, a bulk measurement, indicate that copaiba oil caused a substantial increase in the total volume occupied by the coatings. This result may be related to the surface coverage of the anatomical pores in vegetable ivory, which contribute to a high specific area. The dual composition of copaiba oil, containing both polar and nonpolar functional groups, promoted a compatibilization between silicone oil and the polysaccharide substrate, allowing the penetration of the liquid into the pores during plasma treatment. The same effect did not occur for mulateiro extract due to the lower affinity with silicone oil. As a consequence, the precursor liquid was crosslinked on the particle external surface, resulting in a lower surface coverage and exerting a reduced effect on bulk transfer properties.

The results demonstrate that the reduction in hygroscopicity obtained after the plasma treatment in silicone oil can be further improved by mixing the precursor with copaiba oil, improving the surface coverage of anatomical pores in vegetable ivory microparticles. In contrast, the same result could not be achieved for mulateiro extract, due to its polar character. We hereby show that natural, plant-derived precursors with intermediate polarity can be used

as compatibilization agents between hydrophobic precursors and porous hydrophilic particles during liquid phase plasma treatments.

4 CONCLUSION

Air plasma jet processing of vegetable ivory microparticles immersed in silicone oil induces the formation of coatings that mitigate particle water sorption. The reactions occurring in the plasma-liquid interface between air plasma species and siloxane chains from silicone oil form radicals that are distributed by liquid convection and further recombine on the particle surface, forming films that reduce the accessibility to hydroxyl sorption sites. The reduction in water sorption can be enhanced upon mixing silicone and copaiba oils. Copaiba oil presents both polar and nonpolar functional groups, acting as an interfacial agent between silicone oil and the microparticles. As a result, pore surface coverage is increased and a reduction in bulk water sorption was observed. The same result could not be observed for mulateiro extract, owing to a lower affinity with silicone oil and polar composition. Our results highlight plasma activation of liquids as a material processing technique, allowing the hydrophobization of porous, biosourced microparticles. Natural products, such as copaiba oil, can be used to enhance pore surface coverage and reduce water sorption, enabling particle exposure to a wider range of moisture environments.

ACKNOWLEDGMENTS

The authors would like to acknowledge the financial support provided by Brazilian National Council for Scientific and Technological Development (CNPq, Grant 141665/2019-0), Coordination for the Improvement of Higher Education Personnel (CAPES, Grant 88887.568965/2020-00) and Carlos Chagas Filho Foundation for Research Support of the State of Rio de Janeiro (FAPERJ, Grant 202.350/2022). Communauté Urbaine du Grand

Reims, Département de la Marne, Région Grand Est and European Union (FEDER Champagne-Ardenne 2014-2020) are acknowledged for their financial support to the Chair of Biotechnology of CentraleSupélec and the Centre Européen de Biotechnologie et de Bioéconomie (CEBB).

AUTHOR CONTRIBUTIONS

Yuri Ferreira da Silva: Conceptualization, Investigation, Visualization, Writing – Original Draft. **Giana Almeida:** Conceptualization, Supervision, Resources, Writing – Review & Editing. **Anderson Thiago Vasconcelos Veiga:** Methodology, Writing – Review & Editing. **Renata Nunes Oliveira:** Conceptualization, Supervision, Resources, Writing – Review & Editing. **Patrick Perré:** Conceptualization, Supervision, Funding acquisition, Project administration, Resources, Writing – Review & Editing. **Renata Antoun Simao:** Conceptualization, Supervision, Funding acquisition, Project administration, Resources, Writing – Review & Editing.

CONFLICT OF INTEREST

The authors declare no financial or commercial conflict of interest.

DATA AVAILABILITY STATEMENT

The data that support the findings of this study are available from the corresponding author upon reasonable request.

REFERENCES

[1] K.S. Gobush, C.T.. Edwards, F. Maisels, G. Wittemyer, D. Balfour, R.D. Taylor, Loxodonta cyclotis. The IUCN Red List of Threatened Species 2021, IUCN Red List. 8235 (2021). https://dx.doi.org/10.2305/IUCN.UK.2021-1.RLTS.T181007989A204404464.en.

[2] K.S. Gobush, C.T.. Edwards, F. Maisels, G. Wittemyer, D. Balfour, R.D. Taylor, Loxodonta africana. The IUCN Red List of Threatened Species 2022 (amended version of 2021 assessment)., 8235 (2022). https://dx.doi.org/10.2305/IUCN.UK.2022-2.RLTS.T181008073A223031019.en.

[3] P.B. C.R. Thouless, H.T. Dublin, J.J. Blanc, D.P. Skinner, T.E. Daniel, R.D. Taylor, F. Maisels, H. L. Frederick, African Elephant Status Report 2016 - An update from the African Elephant Database, IUCN, 2016. https://portals.iucn.org/library/sites/library/files/documents/SSC-OP-060_A.pdf.

[4] S. Hauenstein, M. Kshatriya, J. Blanc, C.F. Dormann, C.M. Beale, African elephant poaching rates correlate with local poverty, national corruption and global ivory price, Nat. Commun. 10 (2019). https://doi.org/10.1038/s41467-019-09993-2.

[5] Y. Chu, M.A. Meyers A, B. Wang, W. Yang, J.-Y. Jung, C.F.M. Coimbra, A Sustainable Substitute for Ivory: the Jarina Seed from the Amazon, Sci. Rep. 5 (2015) 14387. https://doi.org/10.1038/srep14387.

[6] B.W. Baker, R.L. Jacobs, M.-J. Mann, E.O. Espinoza, G. Grein, Identification Guide for Ivory and Ivory Substitutes, 4th Editio, CITES, 2020. https://cites.org/sites/default/files/ID_Manuals/Identification_Guide_for_Ivory_and_Ivory_Substitutes_ENGLISH.pdf.

[7] Y. Ferreira da Silva, V. de M. Queiroz, I.C.S. Kling, B.S. Archanjo, R.N. Oliveira, R.A. Simao, Antibacterial coatings on vegetable ivory obtained by cold plasma jet activation of silicone and copaiba oils, Plasma Process. Polym. 17 (2020) 2000035. https://doi.org/10.1002/ppap.202000035.

[8] Y. Ferreira da Silva, F.S. Alencastro, N.D. de Souza, R.N. Oliveira, R.A. Simao, Investigating the origin of laser-induced fluorescence in mannan-rich Phytelephas macrocarpa seeds before and after thermal aging, Carbohydr. Polym. 308 (2023) 120632. https://doi.org/10.1016/j.carbpol.2023.120632.

[9] S. Ghysels, A. Estrada, L. Vanderhaeghen, D. Rousseau, A. Dumoulin, S. Backx, S. Mangelinckx, F. Ronsse, Levoglucosenone, furfural and levomannosan from mannan-rich feedstock: A proof-of-principle with ivory nut, Chem. Eng. J. 451 (2023) 138486. https://doi.org/10.1016/j.cej.2022.138486.

[10] G. Brokamp, H. Borgtoft Pedersen, R. Montúfar, J. Jácome, M. Weigend, H. Balslev, Productivity and management of Phytelephas aequatorialis (Arecaceae) in Ecuador, Ann. Appl. Biol. 164 (2014) 257–269. https://doi.org/10.1111/aab.12098.

[11] US Protagonists: beautiful jewels that respect animals and environment, Vogue Ital. (2017). https://www.vogue.it/en/news/daily-news/2017/09/12/jewels-luxury-respect-animals-environment-us-protagonists/.

[12] S. Ghysels, A.E. Estrada Léon, M. Pala, K.A. Schoder, J. Van Acker, F. Ronsse, Fast pyrolysis of mannan-rich ivory nut (Phytelephas aequatorialis) to valuable biorefinery products, Chem. Eng. J. 373 (2019) 446–457. https://doi.org/10.1016/j.cej.2019.05.042.

[13] E.J. Carvajal-Barriga, J.-L. Putaux, P. Martín-Ramos, J. Simbaña, P. Portero-Barahona, J. Martín-Gil, Opportunities for Ivory Nut Residue Valorization as a Source of

Nanocellulose Colloidal Suspensions, Gels. 9 (2022) 32. https://doi.org/10.3390/gels9010032.

[14] T.E. Timell, Vegetable Ivory as a Source of Mannan Polysaccharide, Can. J. Chem. 35 (1957) 333–338. https://doi.org/10.1139/v57-048.

[15] LUSH Retail Ltd., Tagua Nut Powder - Phytelephas aequatorialis, (n.d.). https://www.lush.com/uk/en/i/tagua-nut-powder.

[16] Sosa export, Phytelephas Aequatorialis Seed Powder, (n.d.). https://sosa-export.com/tagua-white-exfoliant-available-worldwide/.

[17] R. Zhou, R. Zhou, P. Wang, Y. Xian, A. Mai-Prochnow, X. Lu, P.J. Cullen, K. (Ken) Ostrikov, K. Bazaka, Plasma-activated water: generation, origin of reactive species and biological applications, J. Phys. D. Appl. Phys. 53 (2020) 303001. https://doi.org/10.1088/1361-6463/ab81cf.

[18] S. Pan, M. Xu, L. Gan, S. Zhang, H. Chen, D. Liu, Y. Li, X. Lu, Plasma activated radix arnebiae oil as innovative antimicrobial and burn wound healing agent, J. Phys. D. Appl. Phys. 52 (2019). https://doi.org/10.1088/1361-6463/ab234c.

[19] X. Zou, M. Xu, S. Pan, L. Gan, S. Zhang, H. Chen, D. Liu, X. Lu, K.K. Ostrikov, Plasma Activated Oil: Fast Production, Reactivity, Stability, and Wound Healing Application, ACS Biomater. Sci. Eng. 5 (2019) 1611–1622. https://doi.org/10.1021/acsbiomaterials.9b00125.

[20] Y. Gao, Z. Liu, S. Wang, B. Pang, D. Xu, D. Liu, M.G. Kong, The investigation of RONS permeation in plasma- activated oil–water mixed system, Plasma Process. Polym. 18 (2021) 2100038. https://doi.org/10.1002/ppap.202100038.

[21] J.A.S. Ting, L.M.D. Rosario, H. V. Lee, H.J. Ramos, R.B. Tumlos, Hydrophobic coating on glass surfaces via application of silicone oil and activated using a microwave atmospheric plasma jet, Surf. Coatings Technol. 259 (2014) 7–11. https://doi.org/10.1016/j.surfcoat.2014.08.008.

[22] C. Wang, X. He, Preparation of hydrophobic coating on glass surface by dielectric barrier discharge using a 16 kHz power supply, Appl. Surf. Sci. 252 (2006) 8348–8351. https://doi.org/10.1016/j.apsusc.2005.11.042.

[23] Z. Fang, Y. Qiu, E. Kuffel, Formation of hydrophobic coating on glass surface using atmospheric pressure non-thermal plasma in ambient air, J. Phys. D. Appl. Phys. 37 (2004) 2261–2266. https://doi.org/10.1088/0022-3727/37/16/007.

[24] J. Xu, C. Zhang, T. Shao, Z. Fang, P. Yan, Formation of hydrophobic coating on PMMA surface using unipolar nanosecond-pulse DBD in atmospheric air, J. Electrostat. 71 (2013) 435–439. https://doi.org/10.1016/j.elstat.2012.12.011.

[25] P.J. Bruggeman, M.J. Kushner, B.R. Locke, J.G.E. Gardeniers, W.G. Graham, D.B. Graves, R.C.H.M. Hofman-Caris, D. Maric, J.P. Reid, E. Ceriani, D. Fernandez Rivas, J.E. Foster, S.C. Garrick, Y. Gorbanev, S. Hamaguchi, F. Iza, H. Jablonowski, E. Klimova, J. Kolb, F. Krcma, P. Lukes, Z. Machala, I. Marinov, D. Mariotti, S. Mededovic Thagard, D. Minakata, E.C. Neyts, J. Pawlat, Z.L. Petrovic, R. Pflieger, S. Reuter, D.C. Schram, S. Schröter, M. Shiraiwa, B. Tarabová, P.A. Tsai, J.R.R. Verlet,

T. von Woedtke, K.R. Wilson, K. Yasui, G. Zvereva, Plasma–liquid interactions: a review and roadmap, Plasma Sources Sci. Technol. 25 (2016) 053002. https://doi.org/10.1088/0963-0252/25/5/053002.

[26] V. Montano, A. Smits, S.J. Garcia, The bio-touch: Increasing coating functionalities via biomass-derived components, Surf. Coatings Technol. 341 (2018) 2–14. https://doi.org/10.1016/j.surfcoat.2017.10.073.

[27] A. Loesch- Zhang, A. Geissler, M. Biesalski, Plasma polymerization of biogenic precursors, Plasma Process. Polym. (2023) 1–23. https://doi.org/10.1002/ppap.202300016.

[28] L.P. Fontinele, R.C. de Sousa, V.G.F. Viana, E.A. de O. Farias, E.L. Queiroz, C. Eiras, Norbixin extracted from urucum (Bixa orellana L.) for the formation of conductive composites with potential applications in electrochemical sensors, Surfaces and Interfaces. 13 (2018) 92–100. https://doi.org/10.1016/j.surfin.2018.08.002.

[29] M. Cazzola, S. Ferraris, V. Allizond, C.M. Bertea, C. Novara, A. Cochis, F. Geobaldo, A. Bistolfi, A.M. Cuffini, L. Rimondini, G. Banche, S. Spriano, Grafting of the peppermint essential oil to a chemically treated Ti6Al4V alloy to counteract the bacterial adhesion, Surf. Coatings Technol. 378 (2019) 125011. https://doi.org/10.1016/j.surfcoat.2019.125011.

[30] A. Al-Jumaili, A. Kumar, K. Bazaka, M. V. Jacob, Plant secondary metabolite-derived polymers: A potential approach to develop antimicrobial films, Polymers (Basel). 10 (2018). https://doi.org/10.3390/polym10050515.

[31] S.V. Harb, B.M. Cerrutti, S.H. Pulcinelli, C.V. Santilli, P. Hammer, Siloxane-PMMA hybrid anti-corrosion coatings reinforced by lignin, Surf. Coatings Technol. 275 (2015) 9–16. https://doi.org/10.1016/j.surfcoat.2015.05.002.

[32] C. Coquery, F. Carosio, C. Negrell, N. Caussé, N. Pébère, G. David, New bio-based phosphorylated chitosan/alginate protective coatings on aluminum alloy obtained by the LbL technique, Surfaces and Interfaces. 16 (2019) 59–66. https://doi.org/10.1016/j.surfin.2019.04.010.

[33] F. Wang, T. Xie, W. Zhong, J. Ou, M. Xue, W. Li, A renewable and biodegradable all-biomass material for the separation of oil from water surface, Surf. Coatings Technol. 372 (2019) 84–92. https://doi.org/10.1016/j.surfcoat.2019.05.002.

[34] P. Samyn, Active coating for packaging papers with controlled thermal release of encapsulated plant oils, Surfaces and Interfaces. 32 (2022) 102106. https://doi.org/10.1016/j.surfin.2022.102106.

[35] R. da Trindade, J.K. da Silva, W.N. Setzer, Copaifera of the neotropics: A review of the phytochemistry and pharmacology, Int. J. Mol. Sci. 19 (2018). https://doi.org/10.3390/ijms19051511.

[36] P.L. Tobouti, T.C. de Andrade Martins, T.J. Pereira, M.C.M. Mussi, Antimicrobial activity of copaiba oil: A review and a call for further research, Biomed. Pharmacother. 94 (2017) 93–99. https://doi.org/10.1016/j.biopha.2017.07.092.

[37] H. Peixoto, M. Roxo, H. Koolen, F. da Silva, E. Silva, M. Braun, X. Wang, M. Wink,

Calycophyllum spruceanum (Benth.), the Amazonian “Tree of Youth” Prolongs Longevity and Enhances Stress Resistance in Caenorhabditis elegans, Molecules. 23 (2018) 534. https://doi.org/10.3390/molecules23030534.

[38] A.P.A.B. da Silva, R.M.F. Amorim, R. de Freitas Lopes, M.R.L. Mota, F.M.A. da Silva, H.H.F. Koolen, E.S. Lima, A.M.S. Assreuy, R.M. da Cunha, Calycophyllum spruceanum BENTH ameliorates acute inflammation in mice, J. Ethnopharmacol. 219 (2018) 103–109. https://doi.org/10.1016/j.jep.2018.03.023.

[39] D. Nečas, P. Klapetek, Gwyddion: an open-source software for SPM data analysis, Open Phys. 10 (2012) 181–188. https://doi.org/10.2478/s11534-011-0096-2.

[40] R Core Team, R: A language and environment for statistical computing., R Found. Stat. Comput. Vienna, Austria. (2022). https://www.r-project.org/.

[41] C. Beleites, V. Sergo, hyperSpec: a package to handle hyperspectral data sets in R, (2020). https://github.com/cbeleites/hyperSpec (accessed November 8, 2020).

[42] J.D. Berry, M.J. Neeson, R.R. Dagastine, D.Y.C. Chan, R.F. Tabor, Measurement of surface and interfacial tension using pendant drop tensiometry, J. Colloid Interface Sci. 454 (2015) 226–237. https://doi.org/10.1016/j.jcis.2015.05.012.

[43] Y. Ferreira da Silva, V. de M. Queiroz, I.C.S. Kling, B.S. Archanjo, R.N. Oliveira, R.A. Simao, Antibacterial coatings on vegetable ivory obtained by cold plasma jet activation of silicone and copaiba oils, Plasma Process. Polym. 17 (2020) 1–15. https://doi.org/10.1002/ppap.202000035.

[44] H.D. Chanzy, A. Grosrenaud, R. Vuong, W. Mackie, The crystalline polymorphism of mannan in plant cell walls and after recrystallisation, Planta. 161 (1984) 320–329. https://doi.org/10.1007/BF00398722.

[45] P. Stott, C. Cadarache, F.H. Wilhelmsson, Non-Equilibrium Air Plasmas at Atmospheric Pressure, CRC Press, 2004. https://doi.org/10.1201/9781482269123.

[46] D.Z. Pai, Plasma-liquid interfacial layer detected by in situ Raman light sheet microspectroscopy, J. Phys. D. Appl. Phys. 54 (2021) 355201. https://doi.org/10.1088/1361-6463/ac07e0.

[47] I.L. Semenov, K.-D. Weltmann, D. Loffhagen, Modelling of the transport phenomena for an atmospheric-pressure plasma jet in contact with liquid, J. Phys. D. Appl. Phys. 52 (2019) 315203. https://doi.org/10.1088/1361-6463/ab208e.

[48] T.M. Ho, A. Razzaghi, A. Ramachandran, K.S. Mikkonen, Emulsion characterization via microfluidic devices: A review on interfacial tension and stability to coalescence, Adv. Colloid Interface Sci. 299 (2022). https://doi.org/10.1016/j.cis.2021.102541.

[49] A. Lähdetie, P. Nousiainen, J. Sipilä, T. Tamminen, A.-S. Jääskeläinen, Laser-induced fluorescence (LIF) of lignin and lignin model compounds in Raman spectroscopy, Holzforschung. 67 (2013) 531–538. https://doi.org/10.1515/hf-2012-0177.

[50] S. Yasuhara, J. Chung, K. Tajima, H. Yano, S. Kadomura, M. Yoshimaru, N. Matsunaga, T. Kubota, H. Ohtake, S. Samukawa, Structure-designable method to form super low-k SiOC film (k = 2.2) by neutral-beam-enhanced chemical vapour

deposition, J. Phys. D. Appl. Phys. 42 (2009). https://doi.org/10.1088/0022-3727/42/5/055208.

[51] A. Grill, D.A. Neumayer, Structure of low dielectric constant to extreme low dielectric constant SiCOH films: Fourier transform infrared spectroscopy characterization, J. Appl. Phys. 94 (2003) 6697–6707. https://doi.org/10.1063/1.1618358.

[52] Y. Yuan, C. Ye, H.W. Huang, G.F. Shi, Z.Y. Ning, Structural evolution of silicone oil liquid exposed to Ar plasma, Chinese Phys. B. 19 (2010). https://doi.org/10.1088/1674-1056/19/6/065205.

[53] V. Danilov, H.E. Wagner, J. Meichsner, Modification of polydimethylsiloxane thin films in H2 radio-frequency plasma investigated by infrared reflection absorption spectroscopy, Plasma Process. Polym. 8 (2011) 1059–1067. https://doi.org/10.1002/ppap.201100032.

[54] L.M.D. Rosario, H.J. Ramos, R.B. Tumlos, H. V. Lee, J.A.S. Ting, Hydrophobic coating on glass surfaces via application of silicone oil and activated using a microwave atmospheric plasma jet, Surf. Coatings Technol. 259 (2014) 7–11. https://doi.org/10.1016/j.surfcoat.2014.08.008.

[55] S. Tian, X. Wang, Y. Zhang, Numerical study on interactions of atmospheric plasmas and vegetable oils by reactive molecular dynamic simulations, Plasma Process. Polym. 18 (2021) 2100124. https://doi.org/10.1002/ppap.202100124.

[56] K.S.W. Sing, Reporting physisorption data for gas/solid systems with special reference to the determination of surface area and porosity (Recommendations 1984), Pure Appl. Chem. 57 (1985) 603–619. https://doi.org/10.1351/pac198557040603.

[57] E.T. Engelund, L.G. Thygesen, S. Svensson, C.A.S. Hill, A critical discussion of the physics of wood-water interactions, Wood Sci. Technol. 47 (2013) 141–161. https://doi.org/10.1007/s00226-012-0514-7.

[58] E.J. Quirijns, A.J. van Boxtel, W.K. van Loon, G. van Straten, Sorption isotherms, GAB parameters and isosteric heat of sorption, J. Sci. Food Agric. 85 (2005) 1805–1814. https://doi.org/10.1002/jsfa.2140.

[59] G. Almeida, R. Rémond, P. Perré, Hygroscopic behaviour of lignocellulosic materials: Dataset at oscillating relative humidity variations, J. Build. Eng. 19 (2018) 320–333. https://doi.org/10.1016/j.jobe.2018.05.005.

[60] L. Salmén, P.A. Larsson, On the origin of sorption hysteresis in cellulosic materials, Carbohydr. Polym. 182 (2018) 15–20. https://doi.org/10.1016/j.carbpol.2017.11.005.

[61] I. Solala, R. Bordes, A. Larsson, Water vapor mass transport across nanofibrillated cellulose films: effect of surface hydrophobization, Cellulose. 25 (2018) 347–356. https://doi.org/10.1007/s10570-017-1608-z.

[62] K. Kulasinski, R. Guyer, D. Derome, J. Carmeliet, Water Adsorption in Wood Microfibril-Hemicellulose System: Role of the Crystalline-Amorphous Interface, Biomacromolecules. 16 (2015) 2972–2978. https://doi.org/10.1021/acs.biomac.5b00878.

SUPPORTING INFORMATION

Additional supporting information is available in the online version of this article at the publisher's website or from the author.

Graphical Abstract

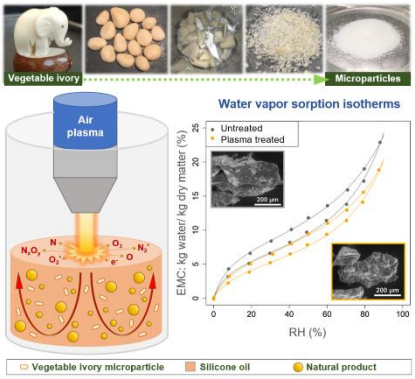

In this study, microparticles of vegetable ivory, a porous and hygroscopic material obtained from Amazonian palm seeds, were treated by an air plasma jet while immersed in silicone oil. As a result, coatings were formed on their surface and a reduction in water vapor sorption was obtained. The reduction in water sorption was enhanced by mixing silicone oil with copaiba oil-resin, which acted as an interfacial agent between silicone oil and the particles during the in-liquid plasma treatment.